Scaling Laws for Melting and Resolidification in Direct Selective Laser Sintering of Metals

Haseung Chung and Suman Das
Department of Mechanical Engineering
University of Michigan
Ann Arbor, MI 48109-2125

Abstract

We present a one-dimensional model describing the physical mechanisms of heat transfer, melting and resolidification taking place during and after the interaction of a laser beam with a semi-infinite metal surface. The physical model describing this situation is based on the classical Stefan problem with appropriately chosen boundary conditions to reflect direct selective laser sintering of metals. A numerical model based on the finite volume method is developed to perform computations for different beam diameters, scan speeds, substrate temperatures and power input profiles. From the results of these computations, we derive relations for time to initiate melting, time to reach maximum melting depth, and total melt-resolidification time. The surface temperature histories for three different power input profiles are compared with approximate closed form solutions.

INTRODUCTION

Direct selective laser sintering (SLS) of metals is a process in which a high-energy laser beam directly consolidates a metal powder or powder mixture to full density. Melting and resolidification processes in direct SLS can have significant effect on the temperature distribution, residual stress, and the final microstructure quality of the parts. Therefore, it is essential to understand the response of melting and resolidification processes to time-dependent changes in heat flux input in order to implement real time laser power, beam diameter, and scan speed control. This is especially necessary to account for process perturbations that occur due to random variations in laser power, for different thermal boundary conditions e.g. whether a layer of powder has a previously solidified layer (conducting) or powder relatively insulating underneath it, as well as to account for variations in thermophysical, optical and material properties when multiple materials are used to make heterogeneous parts.

There are several previous analytical and numerical studies for understanding this kind of phase change problem [1-10]. These studies considered only dynamics of the melting phenomena. However, both melting and resolidification as a function of time-dependent heat flux input are important for real time control of laser fusion based SFF processes. Furthermore, non-dimensional analyses of scaling laws between process variables and controlling parameters in such processes are especially useful in understanding process dynamics. In the future these laws can be incorporated into solidification models that can predict microstructure formation as a function of processing parameters. In this paper, a one-dimensional model that describes the physical mechanisms of heat transfer, melting and resolidification taking place during and after the interaction of a laser beam with a bed of pure metal powder approximated as a semi-infinite surface is presented. We conduct non-dimensional analysis of this process under various conditions.

PHYSICAL MODEL

In this paper, one-dimensional heat conduction with phase change in a solid of length L is considered. Heat flux from a laser flows in through the top surface during heat up while the

322

bottom surface is assumed to be insulated. If heating continues long enough, melting commences and the melt interface moves inward. This is the well documented Stefan problem. After heat flux is turned off, during cool down, heat is lost from the top surface only by radiation. We aim to determine the time to initiate melting, the time to reach maximum melting depth, the total time for melting and resolidification, as well as the temperature distribution, the location and velocity of the melt interface within the domain of interest. The following assumptions are made for developing the model:

- Powder is treated as a solid and no sintering densification occurs during the process.
- Laser beam intensity distribution is uniform across the beam diameter (tophat profile).
- Material properties are independent of temperature in both solid and liquid state.
- No convective heat transfer at top surface (process occurs in a vacuum).
- No melt pool convection, no convective heat transfer at melt interface.
- Planar propagation of melt interface.
- No evaporative heat loss and no evaporative mass transfer at top surface.
- Top surface is diffuse and gray.
- Condition for one-dimensional heat conduction approximation (beam material interaction time $\ll$ radial thermal diffusion time) is met via:

$$\tau_{\text{int}} = \frac{d}{v} \Big/ \frac{d^2}{4\alpha} \ll 1 \tag{1}$$

For the simulations, meaningful values of beam diameter and scan speed were selected to satisfy the above conditions. The following non-dimensional variables were defined:

$$\theta = \frac{T - T_\infty}{T_m - T_\infty}, \chi = \frac{x}{r}, \xi = \frac{tv}{d} = \frac{t}{\tau}, \eta = \frac{vr}{\alpha_s}, St = \frac{c_{ps}(T_m - T_\infty)}{\lambda}, D = \frac{\alpha_s}{\alpha_l}, \kappa = \frac{k_s}{k_l} \tag{2}$$

Defining a boundary heat flux factor $B_f = \dfrac{\alpha_a r c_{ps} q''}{k_s \lambda}$ \hfill (3)

and a boundary radiation heat flux factor $R_f = \dfrac{\varepsilon c_{ps} \sigma (T^2 + T_\infty^2)(T + T_\infty)(T_m - T_\infty)}{k_s \lambda}$ \hfill (4)

The governing equations are

$$\frac{\partial^2 \theta}{\partial \chi^2} = \frac{\eta}{2} \frac{\partial \theta}{\partial \xi} \qquad (solid)$$

$$\frac{\partial^2 \theta}{\partial \chi^2} = \frac{\eta}{2} D \frac{\partial \theta}{\partial \xi} \qquad (liquid) \tag{5}$$

with boundary conditions

$$\frac{\partial \theta}{\partial \chi} = -\frac{B_f}{St} + \frac{R_f}{St} \theta \qquad (solid)$$

$$\frac{\partial \theta}{\partial \chi} = -\frac{B_f}{St} \kappa + \frac{R_f}{St} \kappa \theta \quad (liquid) \tag{6}$$

and Stefan condition

$$\frac{\partial \theta}{\partial \chi}\bigg|_s - \frac{1}{\kappa} \frac{\partial \theta}{\partial \chi}\bigg|_l = \frac{\eta}{2St} \frac{\partial \chi}{\partial \xi} \tag{7}$$

NUMERICAL SCHEME AND EXPERIMENTAL PARAMETERS

Widely used methods for phase change problems include enthalpy methods [11], temperature based equivalent heat capacity methods [11] and front tracking schemes [12]. Each method has some disadvantages as well as some advantages. For our problem, a modified front tracking scheme based on the finite volume method was developed. Discretized governing equations were computed using an explicit scheme satisfying stability criteria. Details of this scheme are available elsewhere [13]. The concept of beam-material interaction time (τ) is used to simulate the temporal action of a moving laser beam over a surface area corresponding to one beam diameter. The beam-material interaction time is defined as the time taken by the beam to traverse one beam diameter, and can be used to set the duration for each power input experienced by an area of the surface corresponding to one beam diameter. Numerical computations were conducted for three types of laser power input; step power input, ramp power input and parabolic power input. Step power input implies laser power is constant during τ. Ramp power input implies laser power increases linearly from 0 to full power during τ. Parabolic power input implies laser power increases quadratically for 0 to full power during τ. Computations were also carried out for 10 different beam diameters with 4 different scan speeds for each type of power input. Thus, each type of power input has 40 different beam-material interaction times. In order to investigate the effect of substrate preheat temperature, we used five different initial temperatures. The material properties of Nickel [14] were used for computations. Table 1 shows beam diameters and scan speeds selected for the computations to satisfy the one-dimensional approximation (eq. 1). Other parameter values used for the computations are shown in table 2.

Diameter (μm)	80	100	150	200	250	300	350	400	450	500
Scan speed (m/s)	1.0	1.0	0.5	0.5	0.5	0.5	0.5	0.5	0.5	0.5
	2.5	2.5	0.75	0.75	0.75	0.75	0.75	0.75	0.75	0.75
	5.0	5.0	1.0	1.0	1.0	1.0	1.0	1.0	1.0	1.0
	7.5	7.5	1.25	1.25	1.25	1.25	1.25	1.25	1.25	1.25

Table 1: Parameters used for numerical computations

Domain Size	Number of Nodes	Time Step	Laser Beam Power
5mm	500	1 x 10^{-8} s	1000 W

Table 2: Parameters used for numerical computations II

RESULTS AND DISCUSSION

Characteristics of non-dimensional time to initiate melting ($\tau_i = \alpha t_i / L^2$), time to reach the maximum melting depth ($\tau_{max} = \alpha t_{max} / L^2$), total time for melting and resolidification ($\tau_{tot} = \alpha t_{tot} / L^2$), non-dimensional maximum melting depth ($\chi_{max} = x_{max} / L$), interface location, interface velocity and surface temperature were obtained by performing numerical computations. Results for each of step, ramp and parabolic power input profiles are discussed below.

Case I: Step Power Input

Figure 1 shows that under one-dimensional assumption, for fixed beam diameter, τ_i is independent of τ_{int}, and therefore also of scan speed v. However, we note τ_i is proportional to beam diameter, and therefore inversely proportional to heat flux at fixed laser power. Therefore,

heat flux is the dominating influence on τ_i. This yields an exponential scaling law between τ_i and non-dimensional diameter as shown in figure 2. An exponential fit for the scaling law yields $\tau_i = 1.14 \times 10^{-6} \exp(49.012\, d/L)$. We observe that heat flux is the dominant factor affecting τ_i (this is discussed elsewhere [13]).
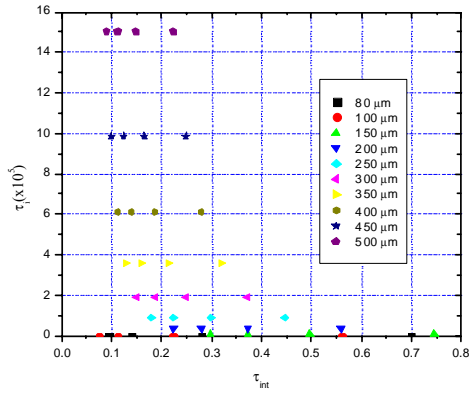
Fig. 1 Non-dimensional time to initiate melting Fig. 2 Non-dimensional time to initiate melting
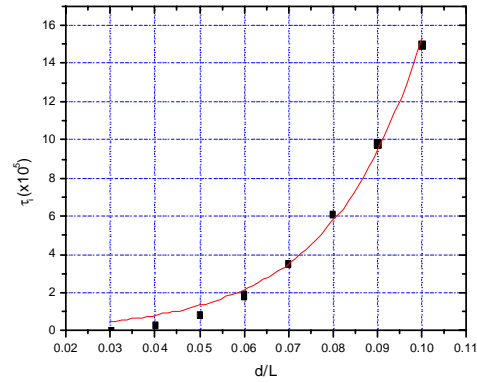
Figure 3 shows that for fixed scan speed, τ_{max} as a function of τ_{int} exhibits a turning point. As beam diameter increases (τ_{int} decreases), τ_{max} decreases to a minimum and then increases. In other words, while τ_{max} is proportional to heat flux up to a certain beam diameter, τ_{max} is proportional to beam material interaction time after that point. Although it is not shown here, total energy dominates τ_{tot} and χ_{max} (this is discussed elsewhere [13]). We can also obtain some relations on the effect of different substrate temperatures. Figure 4 shows τ_i according to different substrate temperatures. As substrate temperature increases, τ_i decreases as expected. In the same manner, scaling laws for τ_{max}, τ_{tot} and χ_{max} as a function of non-dimensional substrate temperature can be also obtained [13].
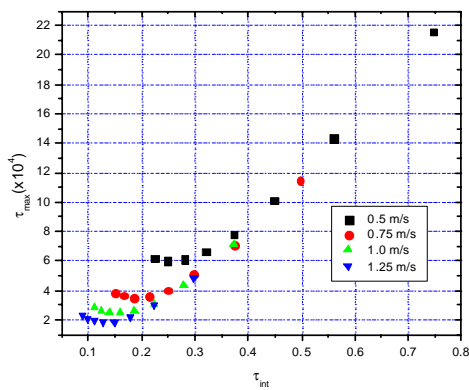
Fig.3 Non-dimensional time to reach maximum melting depth
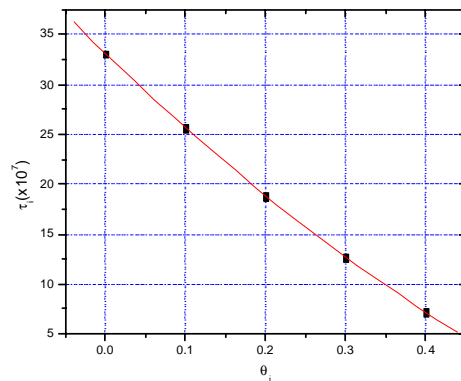
Fig.4 Non-dimensional time to initiate melting
$\tau_i(\times 10^5) = 33.147 - 78.255\theta_t + 33.538\theta_t^2$

Case II: Ramp Power Input

Figure 5 shows a comparison of numerical solution and approximate closed form solution for surface temperature in the case of ramp power input. In the case without melting (figure 5a), both solutions are exactly same but in the case with melting (figure 5b), the numerical solution estimates a higher peak surface temperature compared with Prokhorov's closed form solution [15]. This can be attributed to the lower thermal diffusivity of Nickel in liquid state than that of solid which was considered in our numerical model while the closed form solution assumed constant thermal diffusivity.
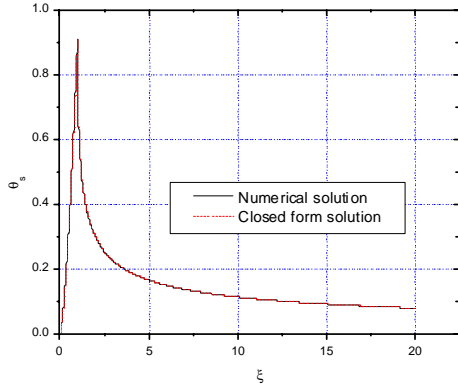
Fig.5(a) Non-dimensional surface temperature (d=500 microns, v=1.0 m/s)
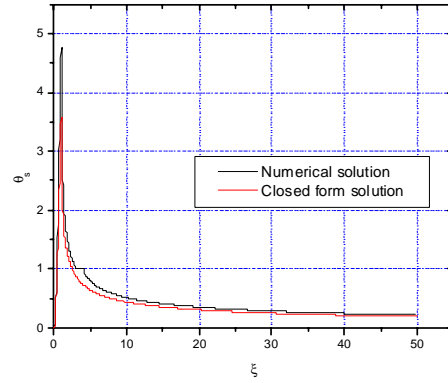
Fig.5(b) Non-dimensional surface temperature (d=200 microns, v=1.0 m/s)

While τ_i is dominated by heat flux in step power input, τ_i is inversely proportional to the slope of power input in ramp power input and τ_{max} is primarily related to τ_{int}, the beam material interaction time [13]. Figure 6 shows that for fixed scan speed, as beam diameter increases (τ_{int} decreases), τ_{max} reaches a minimum and then increases. Therefore, under a fixed scan speed, τ_{max} is a function of heat flux up to a certain point and after that point beam material interaction time dominates τ_{max}. As in the case of step power input, τ_{tot} is primarily dominated by total energy [13]. Figure 7 shows that for fixed scan speed, as beam diameter increases (τ_{int} decreases), τ_{tot} decreases, reaches a minimum and then increases. This implies that for fixed scan speed, total energy dominates τ_{tot} up to a certain point but after that point beam material interaction time has a stronger influence on τ_{tot}. Total energy is also the dominant factor affecting χ_{max} but χ_{max} is proportional to heat flux for same total energy [13].

Scaling laws on the effect of different substrate temperatures were obtained. Figure 8 shows τ_{tot} as a function of non-dimensional substrate temperature. As substrate temperature becomes higher, τ_{tot} increases as expected. The equations for other non-dimensional parameters as a function of non-dimensional substrate temperature were also obtained and are discussed elsewhere [13].
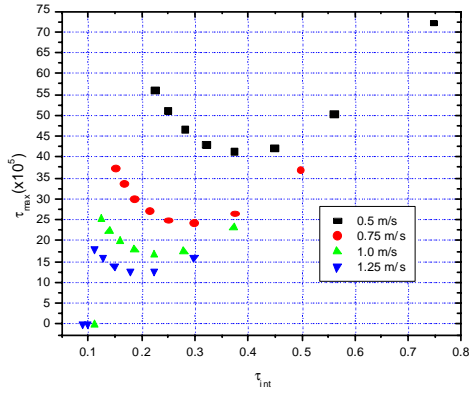
Fig.6 Non-dimensional time to reach maximum melting depth
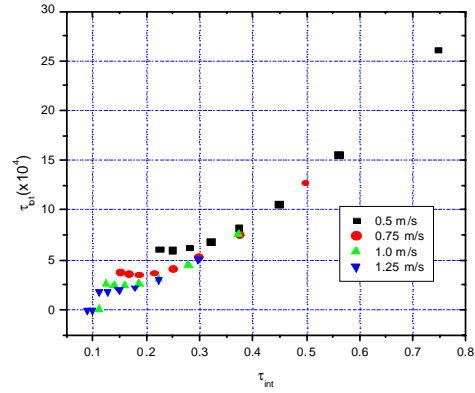
Fig.7 Non-dimensional total time for melting and resolidification
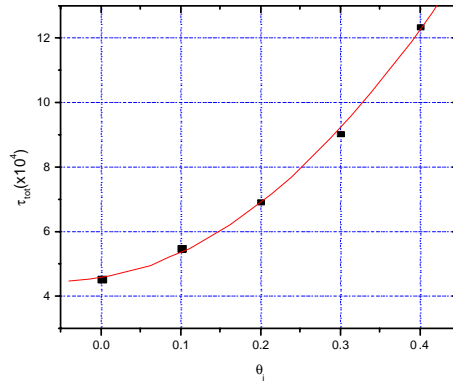
Fig.8 Non-dimensional total time for melting and resolidification
$$\tau_{tot}(\times 10^4) = 4.605 + 3.847\theta_t + 38.239\theta_t^2$$

Case III: Parabolic Power Input

Figure 9 shows comparisons of the numerical and closed form solutions of surface temperature as a function of time for parabolic power input. The two solutions are nearly identical in the case without melting (figure 9a) but for the case with melting (figure 9b), the numerical solution estimates a higher peak surface temperature compared with the closed form solution. This is likely due to change of material properties associated with phase change.

The general trends for parabolic power input are the same as in ramp power input. τ_i is inversely proportional to the slope of power input and τ_{max} is primarily related to τ_{int} . Figure 10 shows that for fixed scan speed, τ_{max} is proportional to heat flux up to a certain point and reaches minimum value. After that point τ_{max} is proportional to beam material interaction time irrespective of heat flux. Therefore, there exists a turning point. Before the turning point heat flux is the dominant factor affecting τ_{max} but after that point beam material interaction time becomes dominant. We note that this turning point shifts to larger τ_{int} compared with ramp power input. τ_{tot} is proportional to beam material interaction time and total energy. Furthermore, χ_{max} is

primarily related with the total energy but for the same total energy χ_{max} is proportional to heat flux (this is discussed elsewhere [13]). Scaling laws on the effect of different substrate temperatures are obtained as in step power input and ramp power input. Figure 11 shows χ_{max} according to different non-dimensional substrate temperatures. As substrate temperature becomes higher, χ_{max} increases as expected. Equations of other non-dimensional parameters as a function of non-dimensional substrate temperature also follow expected trends and are discussed elsewhere [13].
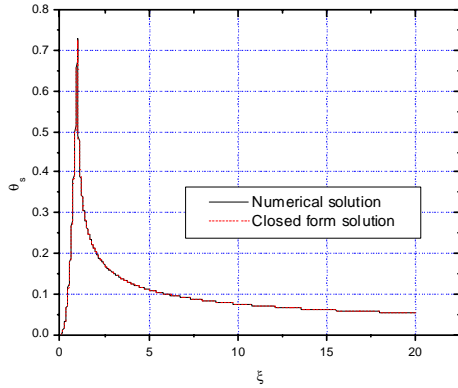
Fig.9(a) Non-dimensional surface temperature (d=500 microns, v=1.0 m/s)
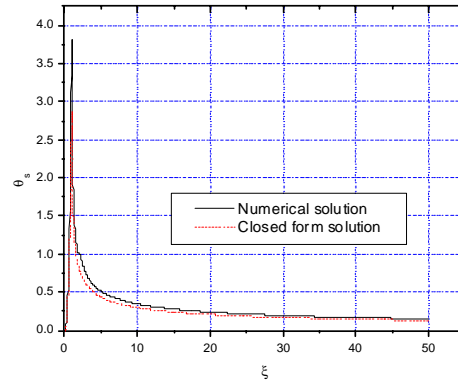
Fig.9(b) Non-dimensional surface temperature (d=200 microns, v=1.0 m/s)
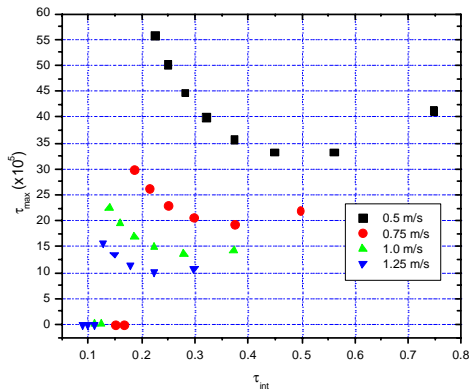
Fig.10 Non-dimensional time to reach maximum melting depth
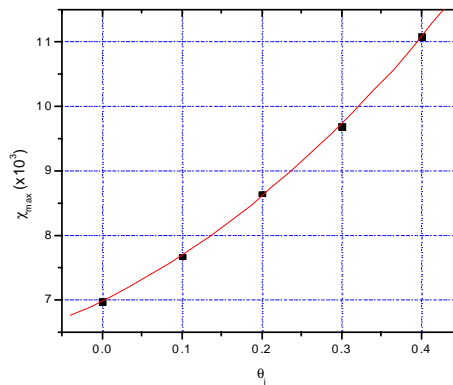
Fig.11 Non-dimensional maximum melting depth
$\chi_{max}(\times 10^3) = 6.986 + 6.056\theta_t + 10.332\theta_t^2$

CONCLUSIONS

Characteristics of non-dimensional time to initiate melting, time to reach the maximum melting depth, total time for melting and resolidification and non-dimensional maximum melting depth were obtained under three different laser power input profiles from the results of this preliminary model. This understanding is helpful to implement effective process control in direct selective laser sintering of metals. Our model will be extended to a moving laser beam in three

dimensions. Future work will also include the effect of powder densification, melt pool convection, melt pool evaporation, surface tension gradients and temperature dependent properties.

REFERENCES
1. Cohen, M. I., 1967, "Melting of a Half-Space Subjected to a Constant Heat Input", Journal of The Franklin Institute, Vol. 283, 1967, pp. 271-285.
2. Zien, T. F., "Integral solutions of Ablation Problems with Time-Dependent Heat Flux", AIAA Journal, Vol.16, 1978, pp. 1287-1295
3. Bertolotti, M., and Sibilia, C., "Depth and Velocity of the Laser-Melted Front from an Analytical Solution of the Heat Conduction Equation", IEEE Journal of Quantum Electronics, Vol. QE-17, 1981, pp. 1980-1988.
4. Sharma, O. P., Rotenberg, M., and Penner, S. S., "Phase-Change Problems with Variable Surface Temperatures", AIAA Journal, Vol. 5, 1967, pp. 677-682
5. Cline, H. E., and Anthony, T. R., "Heat treating and melting material with a scanning laser or electron beam", Journal of Applied Physics, Vol. 48, 1977, pp. 3895-3900.
6. El-Adawi, M. K., and Elshehawey, E. F., "Heating a slab induced by a time-dependent laser irradiance-An exact solution", Journal of Applied Physics, Vol. 60, 1986, pp. 2250-2255.
7. Vujanovic, B. D., and Jones, S. E., "Approximate Solutions of Canonical Heat Conduction Equations", Journal of Heat Transfer, Vol. 112, 1990, pp. 836-842.
8. Xie, J., and Kar, A., "Mathematical modeling of melting during laser materials processing", Journal of Applied Physics, Vol. 81, 1997, pp. 3015-3022.
9. Zhang, Y., and Faghri, A., "Melting and Resolidification of a Subcooled Mixed Powder Bed With Moving Gaussian Heat Source", Journal of Heat Transfer, Vol. 120, 1998, pp. 883-891.
10. Zhang, Y., and Faghri, A., "Melting of a subcooled mixed powder bed with constant heat flux heating", *Int. J. Heat Mass Transfer*, Vol. 42, 1999, pp. 775-788.
11. Cao, Y., and Faghri, A., "A Numerical Analysis of Phase-Change Problems Including Natural Convection", Journal of Heat Transfer, Vol. 112, 1990, pp. 812-816.
12. Alexiades, V., and Solomon, A. D., *Mathematical Modeling of Melting and Freezing Processes*, 1993, Hemisphere Publishing Corporation.
13. Chung, H. and Das, S., "One-Dimensional Numerical Model of Laser-induced Melting and Solidification in Metals" (in press).
14. Touloukian, Y. S., and Ho, C. Y., The TPRC Data Series.
15. Prokhorov, A. M., Konov, V. I., Ursu, I., and Mihailescu, I. N., *Laser Heating of Metals*, 1990, Adam Hilger.

NOMENCLATURE
Symbols
c_p = specific heat (J/kgK)
d = beam diameter (m)
r = beam radius (m)
t = time (sec)
k = thermal conductivity (W/mK)
P = laser power (W)
q'' = heat flux (W/m^2) $\left(= \dfrac{4P}{\pi d^2} \right)$

Greek Letters
α_a = absorptivity of surface
α = thermal diffusivity (m^2/s)
ε = emissivity of surface
λ = latent heat of fusion (kJ/kg)
ρ = density (kg/m^3)
σ = Stefan-Boltzmann constant
θ = Non-dimensional temperature
θ_s = non-dimensional surface temperature

T_m = melting temperature (K)

T_{oo} = ambient temperature (K)

T = temperature at node (K)

x = location within domain (m)

v = beam scan speed (m/s)

D = ratio of thermal diffusivity

St = Stefan number $\left(= \dfrac{c_{ps}(T_m - T_\infty)}{\lambda} \right)$

θ_ι = non-dimensional substrate temperature

ξ = Non-dimensional time

κ = ratio of thermal conductivity

τ = beam material interaction time(=d/v)

η = ratio of beam material interaction time and diffusion time

χ = Non-dimensional length

330